Advanced Multi-rate Kalman Filter for Double Layer State Estimator of Electric Vehicle Based on Single Antenna GPS and Dynamic Sensors

Binh Minh Nguyen* Yafei Wang**
Hiroshi Fujimoto* Yoichi Hori******

**Department of Advanced Energy, the University of Tokyo, Japan,*
(e-mail: minh@hori.k.u-tokyo.ac.jp).

Abstract: In this paper, a double layer state estimator for electric vehicle is proposed. The first layer provides sideslip angle and yaw angle estimation. Utilizing the output the first layer, roll angle, longitudinal and lateral velocity are estimated from the second layer. The estimator is designed by using the course angle and velocity vector obtained from single antenna GPS and a novel advanced multi-rate Kalman filter. While motion control system of electric vehicle requires state estimation every 1 millisecond, the sampling time of GPS based measurement is much longer. In order to solve this problem, inter-sample residual prediction is proposed. Furthermore, by treating the combination of model uncertainties and external disturbances as extended state to be estimated, the high robustness of vehicle state estimation is achieved. The satellite information is utilized for auto-tuning of GPS measurement noise covariance matrix.

Keywords: electric vehicle, global positioning system, Kalman filter, state estimation.

1. INTRODUCTION

The remarkable advantages of in-wheel motor open a new era of novel motion control for electric vehicles (EVs) (Hori, 2004). The big challenge in implementation of EVs' motion control is how to accurately obtain the vehicle states. The sideslip angle is the key state for electronics stability control, roll stability control needs roll angle feedback, and slip ratio control requires the longitudinal velocity for slip ratio calculation. However, reliable sensors to measure such kind of vehicle motion information are not available at affordable costs. For instance, the optical sensor produced by Corrsys-Datron is only used for sideslip angle measurement in experiment at research institutes. For maintaining the reasonable cost of general control system, vehicle state estimator plays a very important role.

Since the last decade, global positioning system (GPS) has been a candidate for vehicle state estimation. Thanks to the Wide Area Augmentation System (WAAS), high accuracy of motion measurements using GPS can be achieved. Japan is developing its own Multi-functional Satellite Augmentation System (MSAS) while Europe has the European Geostationary Navigation Overlay Service (EGNOS). Besides the positions, the attitude (heading angle and course angle) and velocity of a vehicle can be obtained using GPS. By using double antenna GPS receiver, sideslip angle can be calculated directly (Bevly et al., 2006). The main problem of this method is the low update rate of GPS receiver (1-10 Hz) which is not adequate for vehicle motion control (control signal generated at 1 kHz). In order to provide high rate state estimation, the fusion of GPS receiver with other dynamic sensors using Kalman filter has been studied. For instance, sideslip angle can be estimated based on the fusion of single antenna GPS receiver and yaw rate sensor (Anderson et al., 2010). The integration of single antenna GPS and magnetometer introduces a new method for vehicle state estimation (Yoon et al., 2012). Although time delay of GPS measurement was considered, the using of magnetometer increases the cost of this estimation method. In the above two Kalman filter based methods, the robustness of estimation under model uncertainties and external disturbances was not deeply examined. Moreover, due to the long sampling time measurements of GPS, the accuracy of Kalman filter between two continuous updates of GPS measurements is a problem that still remains.

In this paper, novel electric vehicle state estimator using single antenna GPS is proposed. Advance multi-rate Kalman filter is developed as the core theory for the estimator. The long sampling time measurements from GPS (50-200 milliseconds) are combined with short sampling time measurement from other on-board dynamic sensors. Prediction of inter-sample measurement residual is proposed in order to improve the estimation performance during inter-samples (between to continuous updates of GPS measurements). By treating the combination of model uncertainties and external disturbances as extended states, high robustness of state estimation is achieved. By utilizing the number of satellites in view and the dilution of precision, measurement covariance matrix can be tuned in real-time. In this paper the pitch motion is neglected but almost the key states for vehicle motion control are estimated. The estimator has two layers: sideslip angle and yaw angle in the first estimation layer while roll angle, longitudinal velocity and lateral velocity in the second layer.

2. EXPERIMENTAL ELECTRIC VEHILCE

A one seat micro EV named “Super capacitor COMS” is used for this research (Fig. 1). An optical sensor produced by Corrsys-Datron is installed in the front of vehicle. It can provide the measurement of sideslip angle, longitudinal velocity, and lateral velocity for comparing with the estimated values. Four stroke suspension sensors produced by Midori Precisions Co., Ltd. are installed in the suspension system of each wheel. Roll angle is calculated based on the difference between the displacement of the left and right side stroke sensors. The dynamic sensors, including yaw rate, roll rate, longitudinal, and lateral acceleration sensors are installed at the center of gravity of the vehicle. A Linux PC is used as the controller of the experimental vehicle. The control system has the basic sampling time of 1 millisecond. GPS receiver CCA-600 is supported by Japan Radio Co., Ltd. It can provide the measurement of course angle at 5 Hz update rate, with the accuracy of 0.14 degree RMS. The velocity measurement from GPS receiver is provided at the same rate, with the accuracy of 5 cm/s. CCA-600 is integrated with other dynamic sensors for vehicle state estimation. A real-time kinematic GPS receiver, the Hemisphere R320 OmniSTAR, is used for evaluating the accuracy of CCA-600. It can provide the position in real time with the centimetre-level accuracy at 20 Hz update rate. In order to transfer the data from GPS receiver to the controller, we designed GPS interface software (Fig. 2). A laptop with GPS software is used for decoding the NMEA messages from GPS receiver through serial port. The decoded data is sent to EV’s controller through LAN cable.

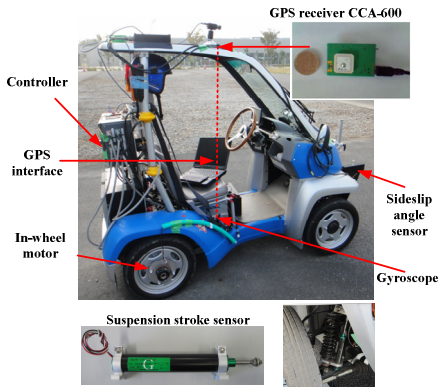

Fig. 1. Experimental setups of “Super-capacitor COMS”.

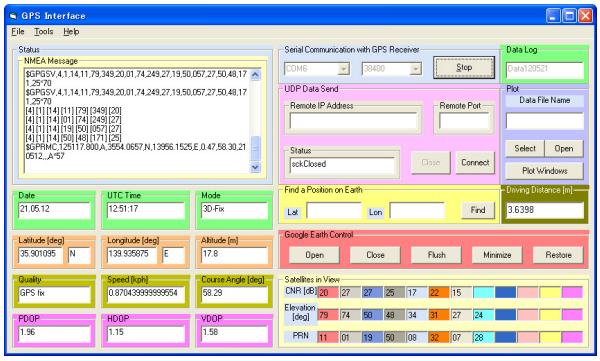

Fig. 2. Interface of GPS software.

3. MODELING OF VEHICLE DYNAMICS

Table 1. Nomenclatures

$\beta,\ \phi$	Sideslip angle, roll angle
V, v_x, v_y	Velocity vector and the longitudinal and lateral component
a_x, a_y	Longitudinal and lateral acceleration
γ, ψ, ν	Yaw rate, yaw angle, and course angle
δ_f, N_z	Front steer angle and yaw moment
C_f, C_r	Front and rear tire cornering stiffness
C_x, K_x	Roll damping and roll spring coefficient
I_z, I_x	Yaw and roll moment of inertia
M, M_s	Total mass and sprung mass of vehicle
h, h_s	Height of CG, distance from CG to roll center
l_f, l_r	Distance from front and rear axle to CG
F_{yf}, F_{yr}	Front and rear lateral force
F_{yd}	Lateral force disturbance
N_{xd}, N_{zd}	Roll moment and yaw moment disturbance

In this paper, the lateral motion is modelled by the planar bicycle model in Fig. 3. The model of roll motion is show in Fig. 4. Here vehicle body is considered as the sprung mass while tires and wheels account for the un-sprung mass. The sprung and un-sprung mass is connected together by suspension system. The following equations express the dynamics of vehicle motion.

$$Mv_x\left(\dot{\beta}+r\right)-M_s h_s\ddot{\phi}=F_{yf}+F_{yr}+F_{yd} \tag{1}$$

$$I_z\dot{\gamma}=F_{yf}l_f-F_{yr}l_r+N_z+N_{zd} \tag{2}$$

$$I_x\ddot{\phi}+C_x\dot{\phi}+K_x\phi=M_s h_s a_y+N_{xd} \tag{3}$$

$$\dot{v}_x=a_x+\gamma v_y \tag{4}$$

$$\dot{v}_y=a_y-\gamma v_x-g\phi \tag{5}$$

$$F_{yf}=-2C_f\left(\beta+\frac{l_f}{v_x}\gamma-\delta_f\right) \tag{6}$$

$$F_{yr}=-2C_r\left(\beta-\frac{l_r}{v_x}\gamma\right) \tag{7}$$

$$v_x=V\cos\beta \tag{8}$$

$$v_y=V\sin\beta \tag{9}$$

The relation between course angle (angle between velocity vector and the North direction) and sideslip angle is presented as:

$$\nu=\beta+\psi \tag{10}$$

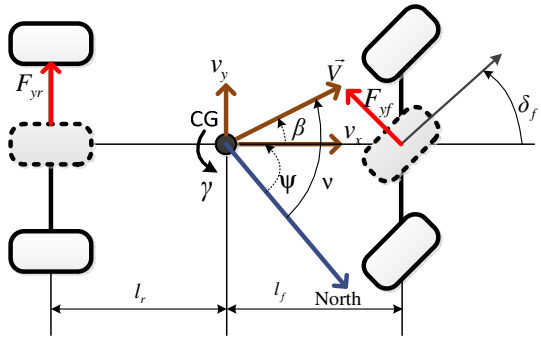

Fig. 3. Planar bicycle model of electric vehicle.

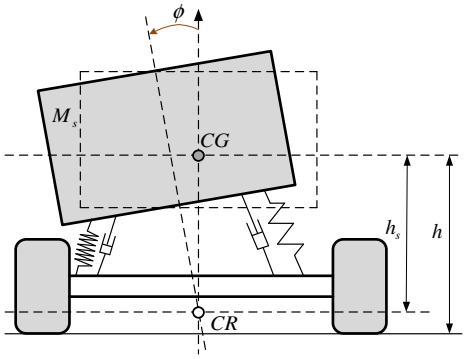

Fig. 4. Roll model of electric vehicle.

4. ADVANCED MULTI-RATE KALMAN FILTER

In this section, the advanced multi-rate Kalman theory is developed to be the core theory of double layer state estimator designed for electric vehicle. This is a special case of Kalman filter such that the sampling time of output measurement is longer than the control period of input signal.

4.1 Disturbance Accommodating

From literature review, disturbance observer (Umeno et al., 1991) and disturbance accommodating control (Johnson, 1971) are well-known method for robust control design. In this paper, the idea of disturbance accommodating is implemented into the Kalman filter for robust state estimation. Considering the following dynamics equation in discrete form:

$$x_{k+1} = \left(A_{dn} + \Delta A_d\right) x_k + \left(B_{dn} + \Delta B_d\right) u_k + d_k + w_k \tag{11}$$

Where the matrix A_{dn} and B_{dn} stands for the nominal model, $\triangle A_d$ and $\triangle B_d$ stands for the model uncertainties and nonlinear parts in the system dynamics, d_k is the external disturbance vector and w_k is the noise vector. Combining the nonlinear parts, model uncertainties and external disturbances, we introduce the unknown input term:

$$d_k^* = \Delta A_d x_k + \Delta B_d u_k + d_k \tag{12}$$

In order to compensate the influence of unknown input term, we treat it as a stochastic process with the dynamics expressed in (13) where w_{dk} is the zero-mean white noise sequence.

$$d_{k+1}^* = d_k^* + w_{d,k} \tag{13}$$

From (11)-(13), the new dynamics equation is defined as follows: $\tilde{X}_{k+1} = \tilde{A}_d \tilde{X}_k + \tilde{B}_d U_k + \tilde{W}_k$

$$\tilde{X}_{k+1} = \tilde{A}_d \tilde{X}_k + \tilde{B}_d U_k + \tilde{W}_k \tag{14}$$

$$\begin{gathered} \tilde{X}_k = \begin{bmatrix} x_k \\ d_k^* \end{bmatrix}, \tilde{U}_k = u_k, \tilde{W}_k = \begin{bmatrix} w_k \\ w_{d,k} \end{bmatrix}, \\ \tilde{A}_d = \begin{bmatrix} A_{dn} & I \\ 0 & I \end{bmatrix}, \tilde{B}_d = \begin{bmatrix} B_{dn} \\ 0 \end{bmatrix} \end{gathered} \tag{15}$$

In the dynamics system (14), the unknown term is accommodated to be extended states. Kalman filter is designed for the system (14) instead of the original system (11). By this way, the unknown term is estimated, thus, the accuracy of state estimation is enhanced.

4.2 Prediction of Inter-sample Measurement Residuals

Analysis of Single-rate Kalman Filter (Ideal Case)

For the sake of simplicity, steady state Kalman filter is used to demonstrate the idea of inter-sample residual prediction. Assume that the output measurement's sampling time is the same as the control period T_c. The discrete model under process noise w_{k-1} and measurement noise v_k is expressed as follows:

$$\begin{aligned} x_k &= A_d x_{k-1} + B_d u_{k-1} + w_{k-1} \\ y_k &= C_d x_k + v_k \end{aligned} \tag{16}$$

The Kalman filter has two stages where L_d is the Kalman gain matrix.

- Prediction stage:

$$\bar{x}_k = A_d \hat{x}_{k-1} + B_d u_{k-1} \tag{17}$$

- Correction stage:

$$\hat{x}_k = \bar{x}_k + L_d \varepsilon_k = \bar{x}_k + L_d \left(y_k - C_d \bar{x}_k\right) \tag{18}$$

Where ε_k is the measurement residual which is updated every T_c in this case. From (16)-(18), the estimation error is derived as:

$$e_k = \left(I - L_d C_d\right) A_d e_{k-1} + \left(I - L_d C_d\right) w_{k-1} - L_d v_k \tag{19}$$

The measurement residual at step k and $k+1$ can be obtained as:

$$\varepsilon_k = C_d A_d e_{k-1} + C_d w_{k-1} + v_k \tag{20}$$

$$\varepsilon_{k+1} = C_d A_d e_k + C_d w_k + v_{k+1} \tag{21}$$

The general formulation of estimation error under noise condition can be expressed as:

$$e_{k+n} = \left[\left(I - L_d C_d\right) A_d\right]^{n+1} e_{k-1} + W_{sr,n} + V_{sr,n} \tag{22}$$

$$W_{sr,n} = \sum_{i=0}^{i=n} \left[\left(I - L_d C_d\right) A_d\right]^{n-i} \left(I - L_d C_d\right) w_{k-1+i} \tag{23}$$

$$V_{sr,n} = -\sum_{i=0}^{i=n} \left[\left(I - L_d C_d\right) A_d\right]^{n-i} L_d v_{k+i} \tag{24}$$

Analysis of Conventional Multi-rate Kalman Filter

Assume that the output measurement's sampling time T_s is longer than the control period T_c. The ratio $r = T_s/T_c$ is defined the multi-rate ratio. In this paper, r is assumed to be an integer. The Kalman filter is designed to provide state estimation every T_c. The estimation steps between two continuous measurement updates are named inter-samples. At step $k = jr$ (j is an integer), the output measurement is updated, thus, the prediction and correction equation is the same as the single-rate case. During inter-samples (at step k = $jr + n$, $n \in [1, r\text{-}1]$), due to the fact that no new measurement is updated, the correction term $L_d\varepsilon_k$ is not accounted in the correction stage. Dynamics of estimation error during inter-samples is derived as follows:

$$e_{k+n} = A_d^n \left[\left(I - L_d C_d\right) A_d\right] e_{k-1} + W_{mr,n} + V_{mr,n} \tag{25}$$

$$W_{mr,n} = A_d^n \left(I - L_d C_d\right) w_{k-1} + \sum_{i=0}^{i=n-1} A_d^{n-i-1} w_{k+i} \tag{26}$$

$$V_{mr,n} = -A_d^n L_d v_k \tag{27}$$

Equation (25) shows that under the influence of model uncertainties and disturbances, during inter-samples, estimation performance may be degraded due to the nonexistence of correction term. The situation will be very serious if matrix A_d introduces the unstable poles into the dynamics of estimation error. This is the algorithm for sideslip angle estimation using GPS and yaw rate sensor (Anderson et al., 2010).

Prediction of Inter-sample Measurement Residual

Fig. 5 explains the key idea of inter-sample measurement residual prediction. When the output measurement update is available, the real measurement residual is used to correct the estimated state. During inter-samples, the predictive measurement residuals are utilized to correct the estimated state. For the simplicity of the algorithm, it is assumed that the process noise and measurement noise can be neglected. From the dynamic equations (16)-(21), the formulation of predictive residual is proposed as follows:

$$\tilde{\varepsilon}_{k+n} = Q_d^n \varepsilon_k, \quad k = jr, \; n \in [1, r-1] \tag{28}$$

Where matrix Q_d is defined in (29).

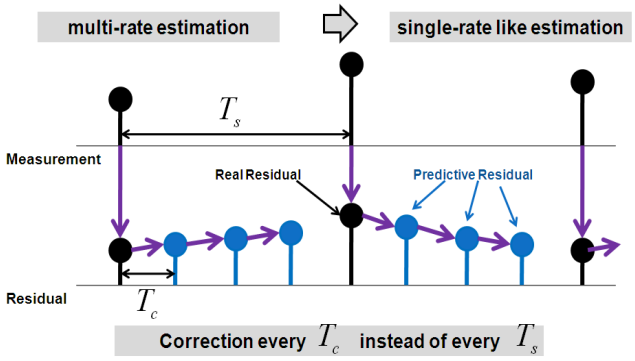

Fig. 5. Idea of inter-sample residual prediction.

By applying (28) for r-1 times during inter-samples, we can prove the following general formulation of estimation error with predictive inter-sample residual:

$$Q_d = C_d A_d \left(I - L_d C_d\right)\left(C_d^T C_d\right)^{-1} C_d^T \tag{29}$$

$$e_{k+n} = \left[\left(I - L_d C_d\right) A_d\right]^{n+1} e_{k-1} + W_{ehmr,n} + V_{ehmr,n} \tag{30}$$

$$W_{ehmr,n} = W_{mr,n} = A_d^n \left(I - L_d C_d\right) w_{k-1} + \sum_{i=0}^{i=n-1} A_d^{n-i-1} w_{k+i} \tag{31}$$

$$V_{ehmr,n} = V_{mr,n} = -A_d^n L_d v_k \tag{32}$$

From (30), the dynamics of estimation error during inter-samples is improved in comparison with the case of conventional multi-rate estimation as expressed in (25). In case of single-rate estimation as in (22), estimation error at any step is driven by the current and the past measurement noise. Therefore, if the system is zero-noise, the proposed method has the same estimation error dynamics as the single-rate estimation. If a big measurement error or strong noise happens at step $k = jr$, the proposed estimation cannot be as good as the single-rate case (ideal case). This is because the error at step $k = jr$ is transferred to every step during inter-samples. Even though, with the proposed method, dynamics of estimation error is better than that of the conventional multi-rate estimation.

4.3 Design of Noise Covariance Matrices

In Kalman filter design, the matrices of process noise covariance (Q_w) and measurement noise covariance (Q_v) are tuning parameters. Small Q_w results in unstable estimation. In contrast, large Q_w will force the estimation to completely rely upon the measurements. The measurement noise covariance matrix is assumed to have the diagonal form:

$$Q_V = \begin{bmatrix} Q_{V\_S} & \\ & Q_{V\_GPS} \end{bmatrix}$$

$$Q_{V\_S} = \begin{bmatrix} \sigma_{S1}^2 & & \\ & \ddots & \\ & & \sigma_{Sn}^2 \end{bmatrix}, Q_{V\_GPS} = \begin{bmatrix} \sigma_{GPS1}^2 & & \\ & \ddots & \\ & & \sigma_{GPSm}^2 \end{bmatrix} \tag{33}$$

$Q_{V\text{-}S}$ is the noise covariance matrix of the conventional sensors, such as yaw rate or lateral acceleration. $Q_{V\text{-}GPS}$ is the noise covariance matrix of the measurements obtained from GPS, such as course angle or velocity. The noise covariance shows the accuracy of the sensor measurement. While $Q_{V\text{-}S}$ can be consider as constant, $Q_{V\text{-}GPS}$ frequently changes due to the operating condition. In this paper, the tuning of $Q_{V\text{-}GPS}$ in real time is proposed. By checking the NMEA messages from GPS receiver, we can know the number of satellites and the dilution of precision of GPS measurement (DOP). If the number of satellites in view is smaller than four, the GPS measurement is unreliable. In this case, the vehicle states are estimated by other methods instead of using GPS.

According to GPS technology, the relative satellite-receiver geometry plays a major role in accuracy of position estimation. If DOP is smaller than 1, it is the ideal case with highest possible precision. A big value of DOP (for example DOP is above 20) results in poor GPS accuracy. Fig. 6 (a) and (b) demonstrates the poor and good GPS satellite geometry, respectively. Lookup tables are constructed to calculate the measurement noise covariance of course angle and velocity from horizontal dilution of precision (HDOP).

4.4 General Algorithm of Advance Multi-rate Kalman Filter

The advance multi-rate Kalman filter is designed based on the disturbance accommodating model in (14). During inter-samples when GPS based measurement is unavailable, GPS measurement residual is calculated using (28). The GPS measurement noise covariance is updated in real time by using HDOP obtained from GPS receiver and lookup tables. The general algorithm is shown in Fig. 7 in which ε_k^s is the measurement residual of conventional sensors, ε_k^{gps} is the measurement residual of GPS, and $\tilde{\varepsilon}_k^{gps}$ is the predictive measurement residual of GPS.

5. DOUBLE LAYER STATE ESTIMATOR DESIGN

Fig. 8 shows the structure of the state estimator for electric vehicle using single antenna GPS with two layers. Each estimation layer is designed using the advance multi-rate Kalman filter algorithm proposed in the previous section. The dynamics model of the first layer is based on the planar bicycle model and GPS model. Long sampling time course angle is combined with short sampling time yaw rate as output measurement. In layer 1, the velocity is a time varying parameter instead of vehicle state. For the simplicity of algorithm, the velocity of non-driven wheel is used as approximate measurement of longitudinal velocity. From the first layer, the yaw angle and sideslip angle is estimated. From the estimated sideslip angle and the velocity from GPS receiver and by using (8) and (9), pseudo measurement of longitudinal and lateral velocity can be calculated at the long sampling time T_s. They are combined with the short sampling time roll rate as multi-rate measurements for the second estimation layer. From this layer, the estimation of roll angle, longitudinal and lateral velocity is achieved.

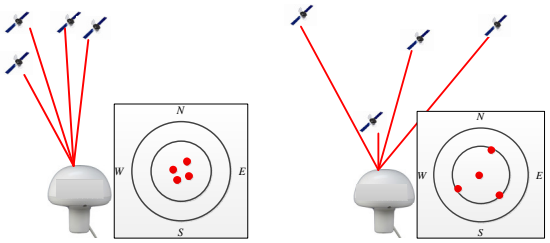

(a) (b)

Fig. 6. GPS satellites with poor DOP (a) and good DOP (b).

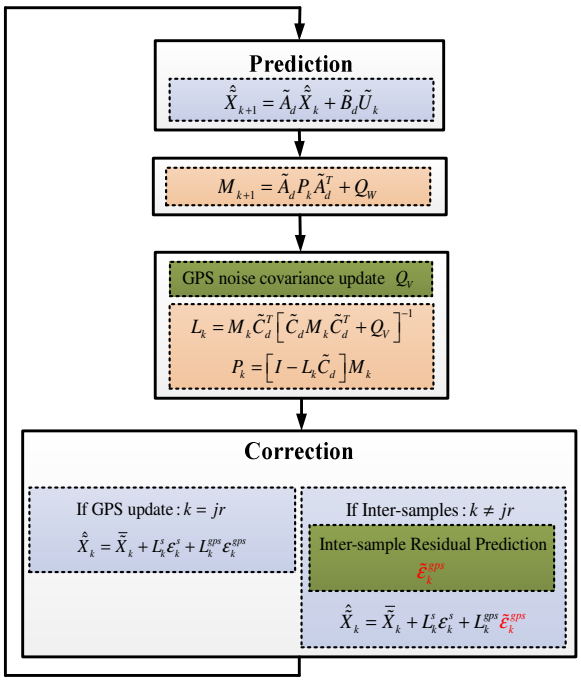

Fig. 7. General algorithm of advance multi-rate Kalman filter for vehicle state estimation using GPS.

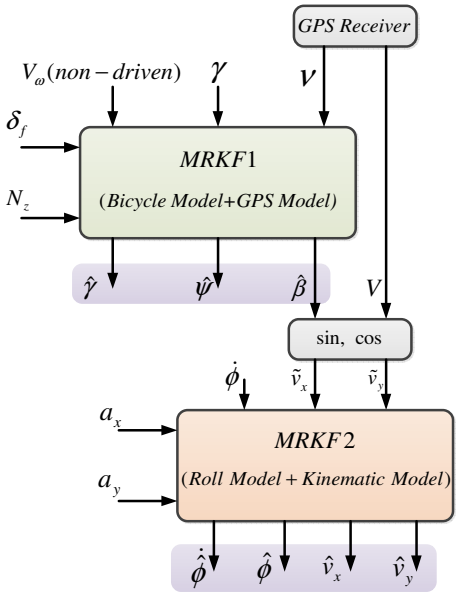

Fig. 8. Double layer state estimator using GPS.

5.1 Estimation model for layer 1

The following equations express the estimation model of layer 1 in which T_c is the short sampling time or the basic sampling time of the system. The course angle obtained from GPS is sampled at long sampling time T_s.

$$\begin{aligned}\tilde{X}_{k+1} &= \begin{bmatrix} A_{dn} & I \\ 0 & I \end{bmatrix}\tilde{X}_k + \begin{bmatrix} B_{dn} \\ 0 \end{bmatrix}U_k + \tilde{W}_k \\ \tilde{Y}_k &= \tilde{C}_d\tilde{X}_k + \tilde{V}_k\end{aligned} \tag{34}$$

$$\tilde{X}_k = \begin{bmatrix} \beta_k & \gamma_k & \psi_k & d_{1,k} & d_{2,k} \end{bmatrix}^T \tag{35}$$

$$\tilde{U}_k = \begin{bmatrix} \delta_{f,k} & N_{z,k} \end{bmatrix}^T \tag{36}$$

$$\tilde{Y}_k = \begin{bmatrix} \gamma_k & v_k \end{bmatrix}^T \tag{37}$$

In (35), the disturbance terms stands for the influence of roll motion to lateral motion, the variation of cornering stiffness, and the external disturbances. The matrices for establishing the nominal estimation model (discrete-time system model) are presented as:

$$A_{dn} = \begin{bmatrix} \frac{-2(C_{fn}+C_{rn})}{Mv_x} & -1-\frac{2(C_{fn}l_f - C_{rn}l_r)}{Mv_x^2} & 0 \\ \frac{-2(C_{fn}l_f - C_{rn}l_r)}{I_z} & \frac{-2(C_{fn}l_f^2 + C_{rn}l_r^2)}{I_z v_x} & 0 \\ 0 & 1 & 0 \end{bmatrix}\times T_c + I_{3\times 3}$$

$$B_{dn} = \begin{bmatrix} \frac{2C_{fn}}{Mv_x} & 0 \\ \frac{2C_{fn}l_f}{I_z} & \frac{1}{I_z} \\ 0 & 0 \end{bmatrix}\times T_c \text{ and } \tilde{C}_d = \begin{bmatrix} 0 & 1 & 0 & 0 & 0 \\ 1 & 0 & 1 & 0 & 0 \end{bmatrix} \tag{38}$$

5.2 Estimation model for layer 2

The model for estimation layer 2 has the same form as (34). The pseudo measurements are sampled at long sampling time T_s. Roll rate, longitudinal and lateral acceleration has the short sampling time of T_c. The following equations express the estimation model of layer 2. In this model, the disturbance terms stand for the uncertainties and variation in roll model, and the influence of roll moment disturbance. According to the kinematic observer (Chen et al., 2008), if the yaw rate is smaller than a threshold value, lateral velocity is unobservable because it used only one measurement of longitudinal velocity. By the using of pseudo measurements of both lateral and longitudinal velocity and by the combination of roll model with kinematic model, the proposed estimation is observable even when yaw rate is close or equal to zero. This is the advantages of the proposed method in comparison with the kinematic observer.

$$\tilde{X}_k = \begin{bmatrix} v_{x,k} & v_{y,k} & \phi_k & \dot{\phi}_k & d_k \end{bmatrix}^T \tag{39}$$

$$\tilde{U}_k = \begin{bmatrix} a_{x,k} & a_{y,k} \end{bmatrix}^T \tag{40}$$

$$\tilde{Y}_k = \begin{bmatrix} \tilde{v}_{x,k} & \tilde{v}_{y,k} & \dot{\phi}_k \end{bmatrix}^T \tag{41}$$

$$A_{dn} = \begin{bmatrix} 0 & \gamma & 0 & 0 \\ -\gamma & 0 & -g & 0 \\ 0 & 0 & 0 & 1 \\ 0 & 0 & \frac{-K_{xn}}{I_{xn}} & \frac{-C_{xn}}{I_{xn}} \end{bmatrix}\times T_c + I_{4\times 4}$$

$$B_{dn} = \begin{bmatrix} 1 & 0 \\ 0 & 1 \\ 0 & 0 \\ 0 & \frac{M_{sn}h_{sn}}{I_{xn}} \end{bmatrix}\times T_c \text{ and } \tilde{C}_d = \begin{bmatrix} 1 & 0 & 0 & 0 & 0 \\ 0 & 1 & 0 & 0 & 0 \\ 0 & 0 & 0 & 1 & 0 \end{bmatrix} \tag{42}$$

6. EXPERIMENTAL VERIFICATION

6.1 Sideslip angle estimation results

Result of the proposed method is compared with that of other two methods, as shown in Fig. 9(a). The first is the linear two-state observer (Aoki et al., 2005). This observer is designed based on the bicycle model with the observer gains obtained by pole placement. The second method is the combination of linear bicycle model with GPS using Kalman filter (Anderson et al., 2004). It is named three-state multi-rate Kalman filter in this paper. The experiment is performed on the road with cornering stiffness $C_f \approx C_r \approx 7000$ [N/rad]. We intentionally design each estimation model with the nominal values $C_{fn} = C_{rn} = 10{,}000$ [N/rad]. This means that a considerable model error is introduced to the estimator. The results show that under model error, the two-state observer has poorest estimation performance. Thanks to the course angle from GPS, three-state multi-rate Kalman filter has better estimation performance. Fig. 9 (b) shows that when GPS course angle is updated, estimation error is minimized. However, during inter-samples where there is no update of course angle, the estimation relies on only yaw rate measurement. As a result, three-state multi-rate Kalman filter is degraded during inter-samples. Using the proposed method, the estimation performance is improved by predicting of inter-sample course angle residual. Moreover, the influence of model error is compensated by disturbance accommodating method. Thus, the sideslip angle estimated by the proposed method can match with the real sideslip angle measured by the Corrsys-Datron's optical sensor. It can be seen clearly in Fig. 9 (b) that during inter-samples, the double layer estimator has smallest estimation error. The double layer estimator also provides the yaw angle estimation at 1 kHz in comparison with the 5 Hz course angle from GPS (Fig. 9 (c)).

6.2 Roll angle estimation results

A two-state Kalman filter is designed based on the roll motion dynamics for roll angle estimation (Tseng et al., 2003). Two states are roll angle and roll rate while roll rate is only one output measurement. Error of 30% is introduced to the nominal roll motion model as follows:

$$\begin{aligned} I_{xn} &= I_{x\_true} + \Delta I_x = I_{x\_true} + 0.3I_{x\_true} \\ C_{xn} &= C_{x\_true} + \Delta C_x = C_{x\_true} + 0.3C_{x\_true} \\ K_{xn} &= K_{x\_true} + \Delta K_x = K_{x\_true} + 0.3K_{x\_true} \end{aligned} \quad (43)$$

Under model error condition, roll angle estimation from two-state Kalman filter method cannot match with the real roll angle obtained from the stroke suspension sensors. In contrast, the double layer estimator can provide the accurate roll angle estimation, as can be seen in Fig. 9(d). This is because the proposed method uses not only roll rate, but also pseudo measurement of lateral and longitudinal velocity. Moreover, the proposed method can compensate the influence of model error and external disturbance.

6.3 Velocity estimation results

Based on kinematic relationship, a two state Kalman filter is designed for vehicle velocity estimation (Chen et al., 2008). According to this method, the non-driven wheel's velocity is used as the approximate measurement of longitudinal velocity. Longitudinal velocity estimation results are shown in Fig. 9(e) while lateral velocity estimation results are shown in Fig. 9(f), respectively. Under the measurement noise condition and the influence of roll motion to lateral motion, estimation error of lateral velocity using the kinematic-based two state Kalman filter increases considerably. By using the double layer estimator, the influence of roll motion to lateral motion is taken to be accounted. Moreover, thanks to the GPS, pseudo measurement of longitudinal and lateral acceleration is obtained. As a result, the double layer estimator provides accurate estimated values of both longitudinal and lateral velocity.

7. CONCLUSIONS

A novel advanced multi-rate Kalman filter is proposed for designing the state estimator of EV. The following key states for EV motion control can be estimated by using single antenna GPS: sideslip angle, yaw angle, roll angle, longitudinal velocity, and lateral velocity. The paper has three main contributions to Kalman filter theory. Firstly, by introducing the prediction of GPS measurement residual for inter-samples, the performance of multi-rate estimation is improved. Secondly, by applying the idea of disturbance accommodating, the robust state estimation is achieved. Thirdly, the dilution of precision of GPS measurement is utilized for tuning the GPS noise covariance in real time. Experimental results show that even under model error and the influence of disturbances, the proposed method achieves accurate state estimation. In future works, sensor fusion algorithm and integrated chassis control system of EVs will be developed based on the proposed double layer state estimator.

REFERENCES

Anderson, R. and Bevly, D. M. (2004). Estimation of Sideslip Angle Using Model Based Estimator and GPS. *American Control Conference*, Vol. 3, pp. 2122-2127.

Aoki, Y., Uchida, T., and Hori, Y. (2005). Experimental Demonstration of Body Slip Angle Control Based on a Novel Linear Observer for Electric Vehicle. *Annual Conference of the IEEE Industrial Electronics Society*, pp. 2620-2625.

Bevly, D. M., Ryu, J., and Gerdes, J. C. (2006). Integrating INS Sensors with GPS Measurements for Continuous Estimation of Vehicle Sideslip, Roll, and Tire Cornering Stiffness. *IEEE Transactions on Intelligent Transportation System*, Vol. 7, No. 4, pp. 483-493.

Chen, B. C. and Hsieh, F. C. (2008). Sideslip Angle Estimation Using Extended Kalman Filter. *Vehicle System Dynamics*, Vol. 46, No. 1, pp. 353-364.

Hori, Y. (2004). Future Vehicle Driven By Electricity and Control-Research on 4 Wheel Motored UOT March II. *IEEE Transactions on Industrial Electronics*, Vol. 51, No. 5, pp. 954-962.

Johnson, C. (1971). Accommodation of External Disturbances in Linear Regulator and Servomechanism Problem. *IEEE Transactions on Automatic Control*, Vol. 16, No. 6, pp. 535-644.

Tseng, H. E. and Li, X. (2003). Robust Model-based Fault Detection For Roll Rate Sensor. *42nd IEEE Conference on Decision and Control*, pp. 1968-1973.

Umeno, T. and Hori, Y. (1991). Robust Speed Control of DC Servomotors Using Two Degrees-of-freedom Controller Design. *IEEE Transactions on Industrial Electronics*, Vol. 38, No. 5, pp. 363-368.

Yoon, J. H. and Peng, H. (2012). Sideslip Angle Estimation Based on GPS and Magnetometer Measurements. *11th International Symposium on Advanced Vehicle Control* (AVEC), Korea, 2012.

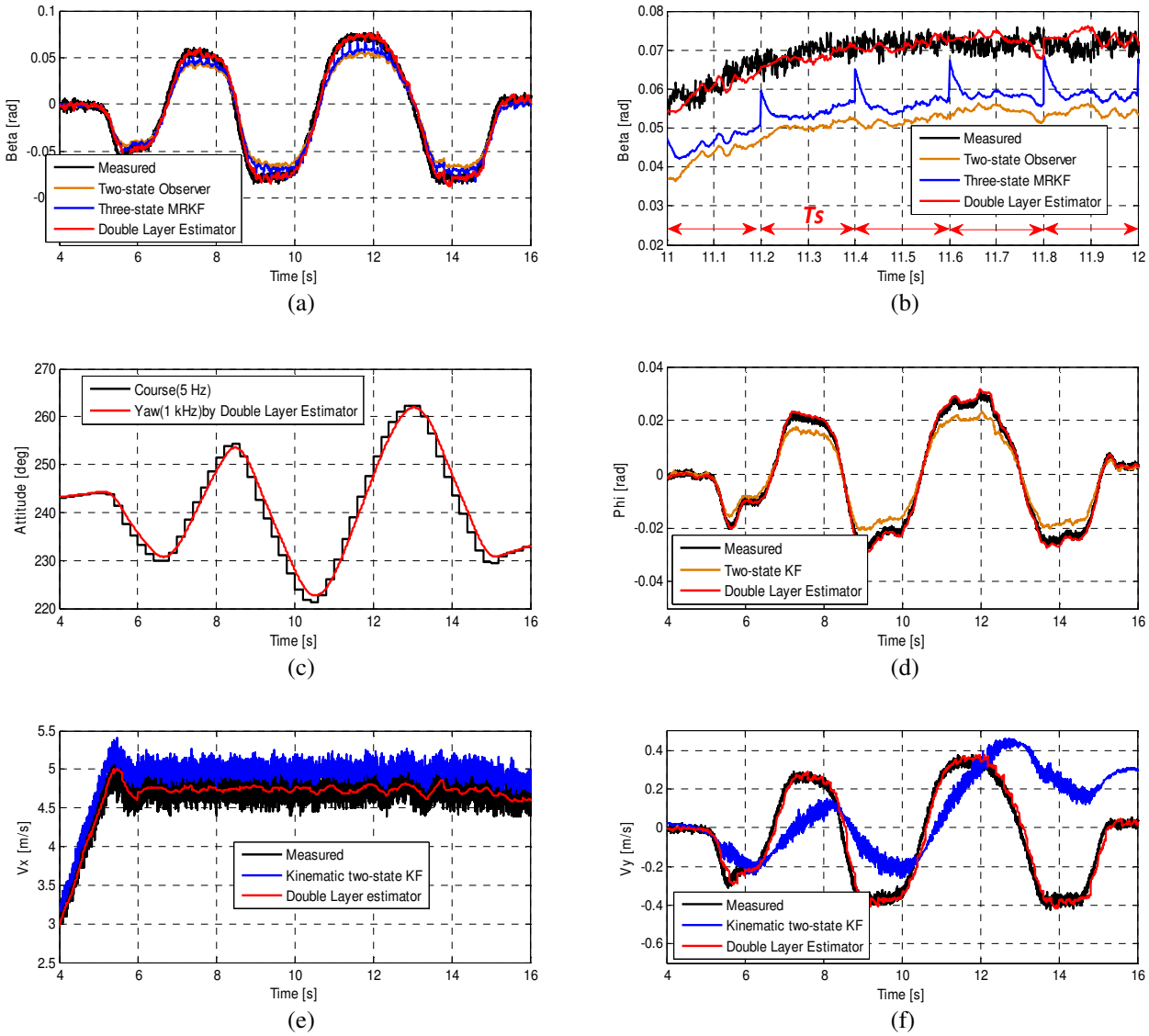

Fig. 9. Estimation results:

(a) sideslip angle, (b) inter-samples of sideslip angle estimation, (c) yaw angle, (d) roll angle, (e) longitudinal velocity, (f) lateral velocity.